

## Accommodation of the carbonate ion in apatite: An FTIR and X-ray structure study of crystals synthesized at 2–4 GPa

MICHAEL E. FLEET,\* XIAOYANG LIU, AND PENELOPE L. KING

Department of Earth Sciences, University of Western Ontario, London, Ontario N6A 5B7, Canada

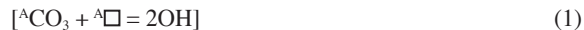
### ABSTRACT

Carbonated hydroxylapatite (C-OHAp) and carbonate apatite (CAp;  $x \geq 0.5$ ) in the composition series  $\text{Ca}_{10}(\text{PO}_4)_{6-y}[(\text{CO}_3)_{x+(3/2)y}(\text{OH})_{2-2x}]$ ,  $x = 0.0\text{--}0.7$ ,  $y = 0.0\text{--}0.6$ , have been synthesized at 2–4 GPa, and studied by FTIR spectroscopy and single-crystal X-ray diffraction. Three structural locations for the carbonate ion have been identified: (1) apatite channel, oriented with two oxygen atoms close to the  $c$ -axis (type A1); (2) close to a sloping face of the  $\text{PO}_4$  tetrahedron (type B); and, (3) stuffed channel position (type A2). Type A1 and B carbonate are equivalent to type A and B CAp of bone and enamel, whereas type A2 is a high-pressure feature. In type A CAp, ordering of type A1 carbonate within the apatite channel results in space group  $P\bar{3}$ ; all other apatites studied have average structures with  $P6_3/m$  symmetry. Results for three new structures are: type A C-OHAp,  $x = 0.14$ ,  $y = 0.0$ ,  $a = 9.4468(4)$ ,  $c = 6.8806(4)$  Å, and  $R$  (residual index of structure refinement) = 0.025; type B C-OHAp,  $x = 0.0$ ,  $y = 0.17$ ,  $a = 9.4234(2)$ ,  $c = 6.8801(3)$  Å, and  $R = 0.025$ ; and type A-B CAp,  $x = 0.7$ ,  $y = 0.5$ ,  $a = 9.4817(6)$ ,  $c = 6.8843(3)$  Å, and  $R = 0.025$ . A fourth structure analysis suggests that the type A-B CAp exchanges some of its channel carbonate with  $\text{OH}^-$  during room-temperature storage in nujol oil, with  $x$  and  $y$  reduced to 0.6 and 0.4, respectively. Local structural adjustments to accommodate the carbonate ion in the  $c$ -axis channel of OHAp include dilation of the channel, contraction of the  $\text{Ca1O}_n$  polyhedron, and rotation of the  $\text{PO}_4$  tetrahedron about the P-O1 bond. The progressive increase in the  $a$  unit-cell edge length with increase in carbonate content of type A CAp is readily attributed to the dilation of the apatite channel. Carbonate-for-phosphate substitution in OHAp (type B CAp) requires displacement of O3 along  $\pm[001]$  and, thus, results in expansion of  $c$  (and contraction of  $a$ ).

### INTRODUCTION

Carbonate apatite (CAp; or carbonated hydroxylapatite, C-OHAp) is the most important component in bone and dental enamel, and both *in vivo* and *in vitro* mineralization of it are researched actively (e.g., Barralet et al. 1998; Penel et al. 1998; Dowker et al. 1999; Dorozhkin and Epple 2002; Elliott 2002; Gross and Berndt 2002; Suchanek et al. 2002). The structure of hydroxylapatite  $[\text{Ca}_{10}(\text{PO}_4)_6(\text{OH})_2]$ ; OHAp; space group  $P6_3/m$  permits extensive atomic substitution and nonstoichiometry in the Ca, P and channel anion ( $X$ ) positions (Mackie and Young 1973; Mackie et al. 1972; Gunawardane et al. 1982; Hughes et al. 1989; Elliott 1994; Fleet and Pan 1995, 1997; Fleet and Liu 2003, 2004; Fleet et al. 2000a, 2000b; Hughes and Rakovan 2002; Pan and Fleet 2002). For example, the  $c$ -axis channel in the apatite structure is readily adaptable for anion substituents, with hydroxyl-, fluor- (FAp), chlor- and carbonate apatites being commonly encountered both as end-members and in mutual solid solution (Hughes et al. 1989; Elliott 1998, 1994; Hughes and Rakovan 2002; Piccoli and Candela 2002). The carbonate ion may also substitute for the phosphate ion. This substitution gives rise to type B CAp, whereas CAp with the carbonate ion located in the apatite channel is known as type A. These separate structural roles of the carbonate ion in apatite have been established

through extensive study by X-ray diffraction (XRD), chemical analyses, infrared (IR) and Raman spectroscopy, and proton and  $^{13}\text{C}$  NMR spectroscopy techniques (e.g., Elliott 1964; LeGeros et al. 1969; Beshah et al. 1990; Regnier et al. 1994; Comodi and Liu 2000; Suetsugu et al. 1998, 2000; Wilson et al. 1999; Ivanova et al. 2001; Fleet and Liu 2003, 2004). In particular, type A and B carbonate have characteristic IR signatures: the former has doublet bands at about 1540 and 1450  $\text{cm}^{-1}$  (derived from the asymmetric stretching vibration,  $\nu_3$ , of the unconstrained  $\text{CO}_3^{2-}$  ion) and a singlet band at 880  $\text{cm}^{-1}$  (the out-of-plane bending vibration,  $\nu_2$ ), and the latter has these bands at about 1455+, 1410 and 875  $\text{cm}^{-1}$ , respectively. Throughout this paper, “carbonate apatite; CAp” has 50% or more of  $X$  ( $= \text{OH}, \text{F}, \text{Cl}$ ) replaced by the carbonate ion according to substitution schemes like:



In the general formula 3 introduced below, CAp has  $x \geq 0.5$ .

Elliott (1964) deduced from polarized IR spectra that the type A carbonate ion in enamel was oriented with its plane approximately parallel to the  $c$ -axis and the type B carbonate ion in carbonated fluorapatite (CFAp; previously referred to as “francolite”) occupied a sloping (inclined to  $c$ -axis) tetrahedral face of the substituted phosphate ion. Based on XRD powder patterns, the stoichiometric end-member type A CAp

\* E-mail: mfleet@uwo.ca

[Ca<sub>10</sub>(PO<sub>4</sub>)<sub>6</sub>CO<sub>3</sub>] appeared to be pseudo-hexagonal with the monoclinic space group *Pb* (Elliott et al. 1980). Alternatively, Suetsugu et al. (1998, 2000) reported that the space group of type A CAp grown from a carbonate flux at 0.55 kbar was *P6*. The disordered average X-ray structure in Suetsugu et al. (2000) was interpreted and refined to show that the equilateral triangular cluster of the channel carbonate ion was bisected by the *c*-axis (see Fig. 1a). More recently, study of CAp synthesized at high pressure, but with an IR signature similar to that of type A CAp in bone and enamel, revealed the space group *P3* (Fleet and Liu 2003). The type A carbonate ion was ordered along the apatite channel at *z* = 0.5, and oriented with two of its oxygen atoms close to the *c*-axis. Fleet and Liu (2003) referred to this orientation (with a bisector of the CO<sub>3</sub> triangle normal to the *c*-axis) as the “closed” configuration (e.g., Fig. 1b), and contrasted it with the “open” vertical (a bisector parallel to *c*-axis) configuration of the channel carbonate ion in type A CAp studied by Suetsugu et al. (2000). Powder XRD Rietveld structure refinement of a

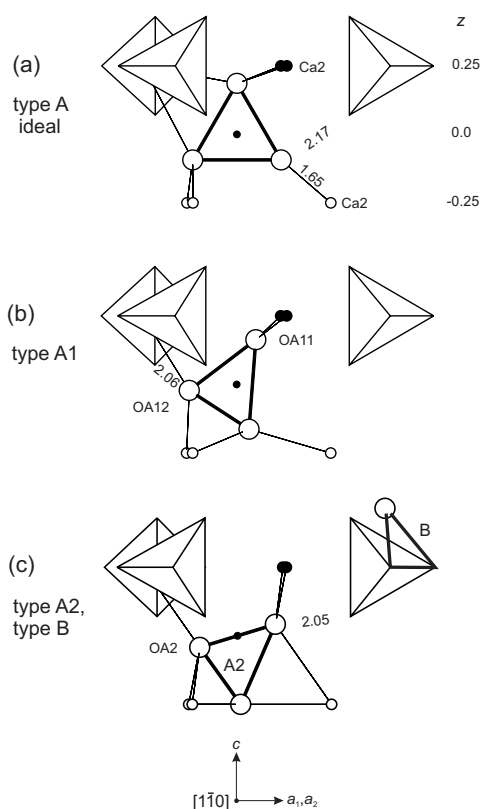


**FIGURE 1.** Part of the *c*-axis channel of hydroxylapatite showing the accommodation of: (a) type A carbonate ion of ideal geometry in upright open (bisector of CO<sub>3</sub> triangle parallel to *c*-axis) configuration with apical oxygen located at the position of OH; (b) closed (bisector normal to *c*-axis) configuration of type A1 carbonate ion in space group *P6<sub>3</sub>/m* (cf., Fleet and Liu 2003); and (c) open (and inverted) type A2 carbonate ion and location of type B carbonate ion close to a sloping face of a substituted PO<sub>4</sub> tetrahedron (Fleet and Liu 2004). OHAp base structure is Sm-bearing OHAp (Fleet et al. 2000a) and extends from *z* = -0.25 to *z* ≈ 0.43; small filled circle is at origin (0, 0, 0) and locates carbon atom in part (a); prohibitively short Ca-O and O-O distances (Å) are indicated; drawn with ATOMS (Dowty 1995).

synthetic Ca-deficient type B CAp (space group *P6<sub>3</sub>/m*) suggested that the type B carbonate ion occupied a vertical (parallel to the *c*-axis) face of the substituted phosphate ion (Ivanova et al. 2001). Very recently, crystals of type A-B CAp (space group *P6<sub>3</sub>/m*) were grown at high pressure in the presence of excess CaCO<sub>3</sub> (experiment PC55; Fleet and Liu 2004). Single-crystal X-ray structural analysis revealed three locations for the carbonate ion: (1) the channel position of the type A carbonate of Fleet and Liu (2003; re-labeled type A1 carbonate); (2) close to a sloping face of the PO<sub>4</sub> tetrahedron and consistent with type B carbonate as characterized by FTIR (Fig. 1c); and (3) a second (stuffed) channel position characterized by IR bands at 1563 and 1506 cm<sup>-1</sup>, which was present in subordinate amounts and appeared to charge-compensate the substitution of PO<sub>4</sub><sup>3-</sup> by CO<sub>3</sub><sup>2-</sup> (type A2 carbonate; Fig. 1c). We presently report on the X-ray structural analysis of type B C-OHAp, type A C-OHAp, and a second preparation of the complex type A-B CAp (high-pressure experiment PC18), interpret the Fourier transform infrared (FTIR) spectra for a wide range in composition of CAp and C-OHAp synthesized at high pressure, and discuss the accommodation of the carbonate ion by the apatite structure. Study of two crystals from PC18 provides independent confirmation of the three structurally distinct locations for carbonate in type A-B CAp and indicates incipient hydroxyl-for-carbonate exchange at room-temperature.

## EXPERIMENTAL PROCEDURES

Single crystals of carbonate apatite and carbonated hydroxylapatite were prepared by direct reaction of stoichiometric amounts of Ca<sub>2</sub>P<sub>2</sub>O<sub>7</sub> (Alfa Aesar; 98%), CaO (Alfa Aesar; 99.95%), and CaCO<sub>3</sub> (Alfa Aesar; 99.99%) at high pressure and temperature in an end-loaded piston-cylinder apparatus. Calcium fluoride (CaF<sub>2</sub>) was added to a single experiment (PC58) for the preparation of carbonated FAp (CFAp). Starting materials were mixed in the proportions indicated in Table 1. Calcium pyrophosphate, CaO, and CaF<sub>2</sub> were dried at 1000 °C, 12 hours, and CaCO<sub>3</sub> at 200 °C, 12 hours. In addition, furnace parts were previously fired at 1000 °C in air. The starting mixture was encapsulated in a sealed platinum tube with a diameter of 5 mm and a height of 12 mm, which was separated by crushable MgO tubing from a graphite tube. The pressure was calibrated from the melting of dry NaCl at 1050 °C (Bohlen 1984) and the quartz coesite transformation at 500 °C (Bohlen and Boettcher 1982). Temperature was measured by inserting a Pt-Pt90%Rh10% thermocouple into the high-pressure cell; it was allowed to fluctuate by about ±5 °C to aid crystal growth. The experiments were initially over-pressurized by about

**TABLE 1.** Synthesis experiments

Experiment	Starting composition*	<i>P</i> (GPa)	<i>T</i> (°C)	Time (hours)	Products†	Reference‡
PC16	9:1	4	1400	5.5	type A C-OHAp + Cc§	3
PC56	9:1	3	1400	5.5	type A CAp + Cc§	3
PC71	9:1	2	1400	6	type A CAp	1
PC74	9:1	2	1500	12	type A CAp	1
PC17	8:2	3	1400	5.5	type B C-OHAp	3
PC55	8:2	3	1400	5.5	type A-B CAp + Cc#	2
PC73	8:2	2	1450	6	type A-B CAp + Cc	3
PC18	7:3	3	1400	5.5	type A-B CAp + melt	3
PC53	7:3	3	1400	5.5		
			1000	13	type A-B CAp + Cc	3
PC57	7:3	3	1400	5.5	type A-B CAp + melt	3
PC59	7:3	3	1500	5.5	type A-B CAp + melt	3
PC26	6:4	2	1350	5.5	type A-B CAp + melt	3
PC58	7:2:1	2	1400	5.5	type B CFAp + melt	3

\* Starting composition is proportion of 1/3(Ca<sub>2</sub>P<sub>2</sub>O<sub>7</sub>+CaO):CaCO<sub>3</sub>:CaF<sub>2</sub>; for PC58 proportion is for 1/3(Ca<sub>2</sub>P<sub>2</sub>O<sub>7</sub>+CaO):CaCO<sub>3</sub>:CaF<sub>2</sub>.

† Melt is carbonate rich.

‡ 1 is Fleet and Liu (2003); 2 is Fleet and Liu (2004); 3 is present study.

§ Trace amounts of calcite (Cc).

# PC55 products were used for annealing experiments at 1000 °C for 15 and 30 minutes, and 12 and 24 hours.

10%, then brought to the correct pressure when the run temperature was attained, and quenched at near-isobaric pressure by switching off the furnace and pumping simultaneously. Run conditions are summarized in Table 1. In Fleet and Liu (2004), aliquots of the products of experiment PC55 were supported on platinum foil and annealed in air at 1000 °C for time intervals ranging from 15 minutes to 24 hours, giving the products PC55-15 and PC55-12 (Table 2). An aliquot of experiment PC17 was annealed similarly for 12 hours in this study.

The products were characterized by optical microscopy, powder XRD (Rigaku D/MAX-B system; CoK $\alpha$  X-radiation), and FTIR spectroscopy (Nicolet Nexus 670 FTIR spectrometer). The infrared spectra were obtained using KBr pellets; 10 mg of carbonate apatite product was diluted in an agate mortar with 1 g of KBr and ground under an infrared heating lamp to a grain size <25  $\mu$ m. Transparent pellets were made under vacuum at a pressure of 200 kg/cm<sup>2</sup>. The high-pressure synthesis experiments yielded apatite crystals up to 300  $\mu$ m in maximum diameter. Trace calcite was evident by optical microscopy in some experiments with the starting proportion 1/3(Ca<sub>2</sub>P<sub>2</sub>O<sub>7</sub>+CaO):CaCO<sub>3</sub> = 9:1, but not detected by either powder XRD or FTIR. The starting proportion of 8:2 resulted in CAp and minor calcite; 7:3 resulted in CAp with about 10% of a carbonate-rich melt, and 6:4 CAp with about 50% melt. The products of PC59 had a lower than expected content of carbonate and eight other experiments (not listed in Table 1) yielded products with low or undetectable amounts of carbonate, results that were attributable variously to loss of CO<sub>2</sub> by baking the starting mixture above 200 °C and failure of the capsule.

Single-crystal fragments were prepared by trimming tablet-shaped grains of apatite with a scalpel blade and evaluated for X-ray structure analysis by optical microscopy and X-ray precession-camera photography. Single-crystal measurements were made at room temperature and pressure with a Nonius Kappa CCD diffractometer and graphite-monochromatized MoK $\alpha$  X-radiation (50 kV, 32 mA,  $\lambda$  = 0.7107 Å). The COLLECT software (Nonius 1997) was used for unit-cell refinement and data collection. The reflection data were processed with SORTAV-COLLECT, using an empirical procedure for absorption correction, and SHELXTL/PC (Siemens 1993). Structure refinements were made with LINEX77 (Coppens 1977). Scattering factors for neutral atomic species and values of the anomalous scattering factors  $f'$  and  $f''$  were taken, respectively, from Tables 2.2A and 2.3.1 of the *International Tables for X-ray Crystallography* (Ibers and Hamilton 1974). Relevant experimental details are given in Tables 2 and 3, final parameters in Table 4, selected bond distances in Table 5, and observed and calculated structure factors in Table 6<sup>1</sup>.

<sup>1</sup>For a copy of Table 6, document item AM-04-071, contact the Business Office of the Mineralogical Society of America (see inside front cover of recent issue) for price information. Deposit items may also be available on the American Mineralogist web site ( or current web address).

## RESULTS AND DISCUSSION

### Interpretation of FTIR spectra

The present study includes ten new synthesis experiments at 2–4 GPa and 1000–1500 °C (Table 1), and extends the investigated starting composition to molar 1/3(Ca<sub>2</sub>P<sub>2</sub>O<sub>7</sub>+CaO):CaCO<sub>3</sub> = 6:4. The results of previous studies, particularly those of Fleet and Liu (2003, 2004), are used as templates for characterizing apatite products from their FTIR spectra (Figs. 2–5). The starting composition for the high-pressure experiments in Fleet and Liu (2003) contained Ca<sub>2</sub>P<sub>2</sub>O<sub>7</sub>, CaO, and CaCO<sub>3</sub> in the molar proportion 1/3(Ca<sub>2</sub>P<sub>2</sub>O<sub>7</sub> + CaO):CaCO<sub>3</sub> = 9:1, and resulted in single-phase type A carbonate apatite (CAp) belonging to the ideal composition series Ca<sub>10</sub>(PO<sub>4</sub>)<sub>6</sub>[(CO<sub>3</sub>)<sub>x</sub>(OH)<sub>2-2x</sub>], with  $x \geq 0.5$  (experiments PC74 and PC71 in Tables 1 and 2). Single-crystal X-ray structural analysis showed that the type A carbonate ion was ordered along the apatite channel at  $z = 0.5$ . Nevertheless, space group  $P\bar{3}$  generates an average CAp structure. Only one carbonate ion centered at  $z = 0.5$  can be accommodated per unit cell, but because all of the carbonate atoms are in general positions, they are disordered in the average structure with multiplicity of six. In spite of the resulting weak electron density of the carbonate atoms, the geometry of the carbonate ion was defined with satisfactory precision. The prominent  $\nu_3$  doublet bands at 1542–1545 and 1456–1459 cm<sup>-1</sup> in the FTIR spectra of these high-pressure synthesized CAp crystals (e.g. PC71 in Fig. 2) closely correspond to the infrared signature of type A carbonate ion in literature studies (e.g. LeGeros et al. 1969; Bonel 1972; Elliott 1994, 2002; Regnier et al. 1994; Barralet et al. 1998). Therefore, it seems probable that type A carbonate in low-temperature natural and precipitated synthetic CAp and bioapatites, and in OHAp, bone and enamel heated in dry CO<sub>2</sub> at 900–1000 °C (LeGeros et al. 1969; Bonel 1972; Elliott 1994; Dowker et al. 1999) also adopts the closed configuration of the  $P\bar{3}$  structure. The closed configuration is also dominant for channel carbonate in type A-B CAp synthesized at 3 GPa from the starting materials mixed in the molar proportion 1/3 (Ca<sub>2</sub>P<sub>2</sub>O<sub>7</sub>+CaO):CaCO<sub>3</sub> = 8:2, resulting in  $\nu_3$  bands at 1541 and 1449 cm<sup>-1</sup>, re-labeled type

**TABLE 2.** Summary of results X-ray structural analysis

Experiment	Crystal	Apatite	Space group	Unit cell		Carbonate content				
						Total CO <sub>3</sub> (wt%)	Formula composition*		Site occupancy ratio	
							x	y	A2/A1	B/A1
<i>a</i> (Å)	<i>c</i> (Å)									
PC17	xt372	B C-OHAp	$P6_3/m$	9.4234(2)	6.8801(3)	1.0	0.0	0.17	–	–
PC16	xt374	A C-OHAp	$P6_3/m$	9.4468(4)	6.8806(4)	0.8	0.14	0.0	–	–
PC74	xt382	A CAp	$P\bar{3}$	9.4917(2)	6.8758(3)	3.0	0.50	0.0	–	–
PC71	xt381	A CAp	$P$	9.5211(3)	6.8725(2)	4.4	0.75	0.0	–	–
PC18†	xt371	A-B CAp	$P6_3/m$	9.4803(3)	6.8853(3)	8.0	0.59	0.41	0.63	0.69
PC18‡	xt373	A-B CAp	$P6_3/m$	9.4817(6)	6.8843(3)	9.2	0.69	0.49	0.57	0.72
PC55	xt376	A-B CAp	$P6_3/m$	9.5143(3)	6.8821(2)	10.6	0.69	0.57	0.82	0.83
PC55-15§	xt383	A-B CAp	$P6_3/m$	9.4931(4)	6.8888(5)	10.4	0.62	0.82	0.52	1.32
PC55-12#	xt377	A-B CAp	$P6_3/m$	9.4716(4)	6.8968(3)	10.3	0.70	0.76	0.40	1.09

Notes: See Table 1 for sources of data and text for calculation procedures.

\* Based on idealized formula Ca<sub>10</sub>(PO<sub>4</sub>)<sub>6-y</sub>[(CO<sub>3</sub>)<sub>x+(3/2)y</sub>(OH)<sub>2-2x</sub>];

individual formulae using total carbonate from A1,A2,B site occupancies are:

PC17- Ca<sub>10</sub>(PO<sub>4</sub>)<sub>5.83</sub>(CO<sub>3</sub>)<sub>0.17</sub>(OH)<sub>2.00</sub>; PC16- Ca<sub>10</sub>(PO<sub>4</sub>)<sub>6.00</sub>(CO<sub>3</sub>)<sub>0.14</sub>(OH)<sub>1.72</sub>; PC74- Ca<sub>10</sub>(PO<sub>4</sub>)<sub>6.00</sub>(CO<sub>3</sub>)<sub>0.50</sub>(OH)<sub>1.00</sub>;  
 PC71- Ca<sub>10</sub>(PO<sub>4</sub>)<sub>6.00</sub>(CO<sub>3</sub>)<sub>0.75</sub>(OH)<sub>0.50</sub>; PC18†- Ca<sub>10</sub>(PO<sub>4</sub>)<sub>5.59</sub>(CO<sub>3</sub>)<sub>1.37</sub>(OH)<sub>0.82</sub>; PC18‡- Ca<sub>10</sub>(PO<sub>4</sub>)<sub>5.51</sub>(CO<sub>3</sub>)<sub>1.57</sub>(OH)<sub>0.62</sub>;  
 PC55- Ca<sub>10</sub>(PO<sub>4</sub>)<sub>5.43</sub>(CO<sub>3</sub>)<sub>1.84</sub>(OH)<sub>0.62</sub>; PC55-15- Ca<sub>10</sub>(PO<sub>4</sub>)<sub>5.18</sub>(CO<sub>3</sub>)<sub>1.76</sub>(OH)<sub>0.76</sub>; PC55-12- Ca<sub>10</sub>(PO<sub>4</sub>)<sub>5.24</sub>(CO<sub>3</sub>)<sub>1.74</sub>(OH)<sub>0.60</sub>;

† Stored in nujol;

‡ Stored dry.

§ Annealed at 1000 °C in air for 15 minutes.

# Annealed at 1000 °C in air for 12 hours.

**TABLE 3.** Experimental details for X-ray structural analysis

Experiment	PC17	PC16	PC18	PC18
			nujol stored	dry stored
Crystal	xt372	xt374	xt371	xt373
Crystal size (mm <sup>3</sup> × 10 <sup>3</sup> )	0.13	0.23	0.49	0.21
Crystal shape	prism	prism	cube	tablet
Formula weight	1003.8	1008.3	1017.5	1019.8
D <sub>x</sub> (g/cm <sup>3</sup> )	3.150	3.148	3.153	3.159
Reflections – unique	561	565	569	570
– number, with (I < 3σ <sub>0</sub> )	264	277	308	252
– R <sub>int</sub> *	0.034	0.035	0.029	0.027
Refined parameters	44	43	57	56
μ* (cm <sup>-1</sup> )	29.2	29.2	28.7	28.6
R†	0.025	0.025	0.025	0.025
R <sub>w</sub> †	0.023	0.024	0.021	0.022
s‡	1.25	1.35	1.19	1.35
Extinction (× 10 <sup>4</sup> )	1.04(7)	0.26(6)	0.51(6)	0.29(6)
Δρ‡ (e/Å <sup>3</sup> ) (+)	0.60	0.58	0.50	0.47
(-)	0.37	0.42	0.39	0.47

\* R<sub>int</sub> is residual index for intensities of equivalent reflections; μ is linear absorption coefficient.

† Least-squares refinement parameters: R is residual index; R<sub>w</sub> is weighted residual index; s is goodness-of-fit.

‡ Δ is residual electron density.

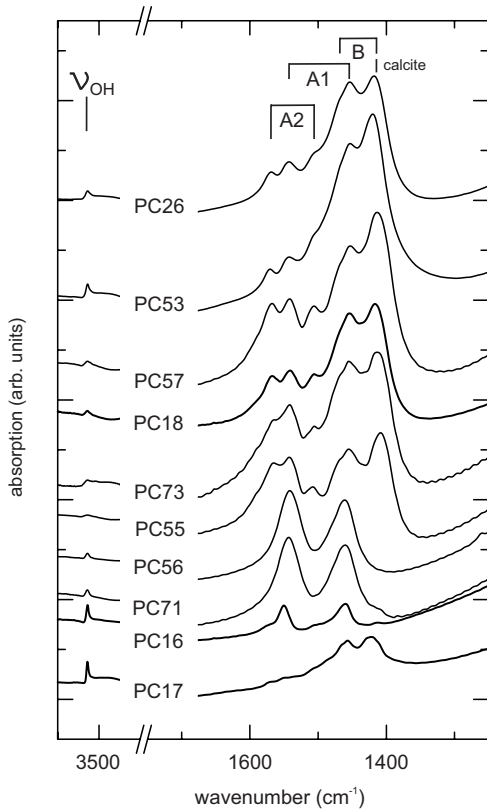


**FIGURE 2.** FTIR spectra of products of piston-cylinder experiments: bands due to OH stretching ( $\nu_{OH}$ ) and asymmetric stretching ( $\nu_3$ ) of type A1, A2, and B carbonate ion are identified; PC17 is type B C-OHAp; PC16 is type A C-OHAp; PC71 and PC56 are type A CAP with P<sup>3</sup> structure; PC55, PC73 and PC53 are type A-B CAP + calcite; and, PC18, PC57 and PC26 are type A-B CAP + quenched melt; the asymmetric stretching ( $\nu_3$ ) vibration of the carbonate ion in single-crystal calcite results in a fairly broad singlet band at 1407 cm<sup>-1</sup>, with measured values for powder samples ranging up to 1435 cm<sup>-1</sup> (White 1974); see Table 1 for experimental details, and Table 2 footnote for apatite formulae.

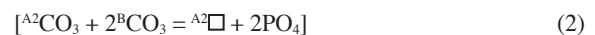
**TABLE 4.** Atomic coordinates and isotropic displacement parameters (Å<sup>2</sup>)

Site occupancy	$U_{eq} = (1/3) \sum_i \sum_j U^i_j a^i a^j$			$U, U_{eq}$	
	x	y	z		
<b>xt372 (PC17)</b>					
Ca1	1.0	2/3	1/3	0.0017(1)	0.0148(5)
Ca2	1.0	0.99304(8)	0.24700(8)	1/4	0.0137(2)
P	0.976(3)	0.3688(1)	0.3988(1)	1/4	0.0101(3)
O1	1.0	0.4845(2)	0.3289(2)	1/4	0.0150(5)
O2	1.0	0.4649(2)	0.5866(2)	1/4	0.0200(6)
O3	0.988	0.2580(2)	0.3432(2)	0.0714(2)	0.0240(4)
O4	0.5	0	0	0.1950(7)	0.023(2)
H	0.72(5)	0	0	0.053*	0.023*
OB3	0.014(3)	0.36*	0.43*	0.47*	0.025*
<b>xt374 (PC16)</b>					
Ca1	1.0	2/3	1/3	0.0018(1)	0.0156(5)
Ca2	1.0	0.99268(8)	0.24830(9)	1/4	0.0158(2)
P	1.0	0.3689(1)	0.3993(1)	1/4	0.0130(3)
O1	1.0	0.4845(2)	0.3287(2)	1/4	0.0151(5)
O2	1.0	0.4649(3)	0.5862(2)	1/4	0.0234(7)
O3	1.0	0.2587(2)	0.3435(2)	0.0710(2)	0.0285(5)
O4	0.5	0	0	0.1949(8)	0.035(3)
H	0.65(6)	0	0	0.53*	0.035*
C	0.01*	0	0	0	0.025*
OA12	0.012(3)	0.944*	0.126*	0.527*	0.025*
<b>xt371 (PC18)</b>					
Ca1	1.0	2/3	1/3	0.0021(1)	0.0179(5)
Ca2	1.0	0.99093(7)	0.24944(8)	1/4	0.0222(2)
P	0.943(3)	0.3708(1)	0.4014(1)	1/4	0.0160(3)
O1	1.0	0.4847(2)	0.3313(2)	1/4	0.0198(5)
O2	1.0	0.4657(2)	0.5856(2)	1/4	0.0368(7)
O3	0.971	0.2608(3)	0.3459(3)	0.0723(3)	0.0430(6)
O4†	0.36(3)	0	0	1/4	0.025*
C	0.26(1)	0	0	0	0.025*
OA11	0.105(4)	0.028(4)	0.998(7)	0.662(3)	0.025*
OA12	0.049(5)	0.953(5)	0.123(4)	0.536(5)	0.025*
OA2	0.062(5)	0.911(5)	0.015(6)	0.461(4)	0.025*
OB3	0.034(4)	0.359(6)	0.435(6)	0.472(8)	0.025*
<b>xt373 (PC18)</b>					
Ca1	1.0	2/3	1/3	0.00210(8)	0.0175(4)
Ca2	1.0	0.99095(7)	0.24961(8)	1/4	0.0214(2)
P	0.941(3)	0.3709(1)	0.4014(1)	1/4	0.0150(3)
O1	1.0	0.4847(2)	0.3310(2)	1/4	0.0190(5)
O2	1.0	0.4658(2)	0.5855(2)	1/4	0.0356(6)
O3	0.971	0.2605(3)	0.3460(3)	0.0727(2)	0.0412(5)
O4†	0.122(6)	0.0142*	0	1/4	0.025*
C	0.22(2)	0	0	0	0.025*
OA11	0.098(3)	0.023(2)	0	0.661(2)	0.025*
OA12	0.057(4)	0.946(3)	0.123(3)	0.525(3)	0.025*
OA2	0.065(4)	0.925(4)	0.021(4)	0.455(3)	0.025*
OB3	0.041(4)	0.348(5)	0.421(5)	0.477(5)	0.025*

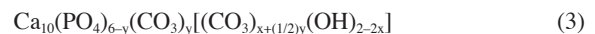
\* Not refined.

† O4 has contributions from both type A2 carbonate and hydroxyl ions.

A1 carbonate ion, for experiment PC55 (Fleet and Liu 2004; see present Fig. 2 and Tables 1 and 2). In addition, the shortfall in phosphate in this experiment resulted in a significant content of type B carbonate ( $\nu_3$  bands at ~1470 and 1406 cm<sup>-1</sup>), and it appeared that the carbonate-for-phosphate substitution was charge balanced largely by the entry of carbonate into a second (stuffed) channel position, characterized in the FTIR spectrum by  $\nu_3$  bands at 1563 and 1506 cm<sup>-1</sup> (type A2 carbonate ion). The idealized substitution scheme and formula for high-pressure CAP were:



and,



respectively. The space group of high-pressure type A-B CAP

**TABLE 5.** Selected bond distances (Å)

	PC17 xt372	PC16 xt374	PC18 xt371	PC18 xt373
Ca1-O1 × 3	2.407(1)	2.409(1)	2.420(1)	2.419(1)
Ca1-O2a × 3	2.458(1)	2.464(2)	2.479(1)	2.479(1)
Ca1-O3a × 3	2.808(2)	2.814(2)	2.809(2)	2.808(2)
Mean	2.558	2.562	2.569	2.569
Ca2-O1b	2.708(2)	2.707(2)	2.716(2)	2.715(2)
Ca2-O2c	2.356(2)	2.350(2)	2.342(2)	2.341(2)
Ca2-O3d × 2	2.510(2)	2.526(2)	2.557(2)	2.554(2)
Ca2-O3e × 2	2.349(1)	2.344(2)	2.352(2)	2.355(1)
Mean	2.464	2.466	2.480	2.479
Ca2-O4	2.391(1)	2.411(1)	2.4089(6)	2.413*
P-O1	1.530(2)	1.537(2)	1.525(2)	1.526(2)
P-O2	1.533(2)	1.529(2)	1.513(2)	1.512(2)
P-O3 × 2	1.526(2)	1.527(2)	1.521(2)	1.521(2)
Mean	1.529	1.530	1.520	1.520

Notes:  $a = 1 - x, 1 - y, -z$ ;  $b = 1 - y, x - y, z$ ;  $c = 1 - x + y, 1 - x, z$ ;  $d = 1 + x, y, z, e = 1 + x - y, x, -z$ .

\* O4 (of type A2 carbonate and OH<sup>-</sup> ions) not on c axis, resulting in three values for Ca2-O4 in the average structure, varying from 2.276 to 2.484 Å.

is  $P6_3/m$ , so that the carbonate oxygen atoms, which are all in general positions, are disordered with multiplicity of twelve. Due to the combined effects of partial occupancy and disorder, the atoms of the three different carbonate ions are represented in the X-ray structural analysis by features considerably weaker than a hydrogen atom. Moreover, the electron density of two of the oxygen atoms of the type B carbonate ion is overwhelmed by that for oxygen atoms of the phosphate group, making their precise location uncertain. Nevertheless, the three different structural locations for the carbonate ion were resolved in Fleet and Liu (2004) and correlated with the FTIR spectra by matching site occupancies from the X-ray structural analysis with relative areas of the asymmetric stretching bands. The type A1 carbonate ion is in the closed (bisector of CO<sub>3</sub> triangle normal to *c*-axis) channel configuration of the  $P\bar{3}$  structure, but now disordered at  $z = 0.0$  and 0.5. The type B carbonate ion is located close to a sloping (inclined to *c*-axis) face of the substituted PO<sub>4</sub> tetrahedron; O1 and O2 are “common” to both carbonate and phosphate ions and the displacement of the third oxygen atom (one of the two O3 atoms) tilts the plane of the carbonate ion away from the P atom vacancy. The type A2 carbonate ion is in an open (bisector parallel to *c*-axis) configuration but rotated about the horizontal axis so that the apical oxygen atom is displaced slightly off the *c*-axis.

In summary, the FTIR spectra (Figs. 2–5) may be used to infer information on OH<sup>-</sup> and CO<sub>3</sub><sup>2-</sup> in the experimental products, in the following manner: (1) the area of the sharp band at ~3570 cm<sup>-1</sup> is proportional to the content of OH<sup>-</sup> in the apatite channel, with PC71 containing about 0.25 (OH)<sub>2</sub> per formula unit (pfu); (2) calcite is characterized by a singlet  $\nu_3$  carbonate asymmetric stretching band at ~1410 cm<sup>-1</sup>; (3) type B carbonate by the doublet of the high-frequency shoulder to the ~1455 cm<sup>-1</sup> band and the band at ~1410 cm<sup>-1</sup>; (4) type A1 carbonate by the doublet of bands at ~1540 and ~1455 cm<sup>-1</sup>; and (5) type A2 carbonate by the doublet of bands at ~1565 and ~1505 cm<sup>-1</sup>. Selected references for these assignments are LeGeros et al. (1969), Bonel (1972), White (1974), Nelson and Featherstone (1982), Vignoles et al. (1988), Regnier et al. (1994), Suetsugu et al. (1998), and Fleet and Liu (2003, 2004). There is, however, ambiguity in assignment

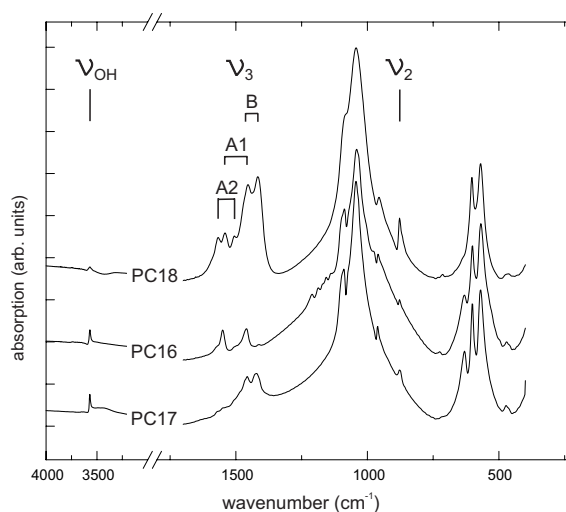


**FIGURE 3.** FTIR spectra for synthesis experiments yielding apatites investigated by X-ray structural analysis in this study, identifying bands due to OH stretching ( $\nu_{OH}$ ) and asymmetric stretching ( $\nu_3$ ) and out-of-plane bending ( $\nu_2$ ) of carbonate ion: PC17 is type B C-OHAp; PC16 is type A C-OHAp; and PC18 is type A-B CAP; note the relatively high content of OH in PC17 and PC16 (see Table 2 footnote).

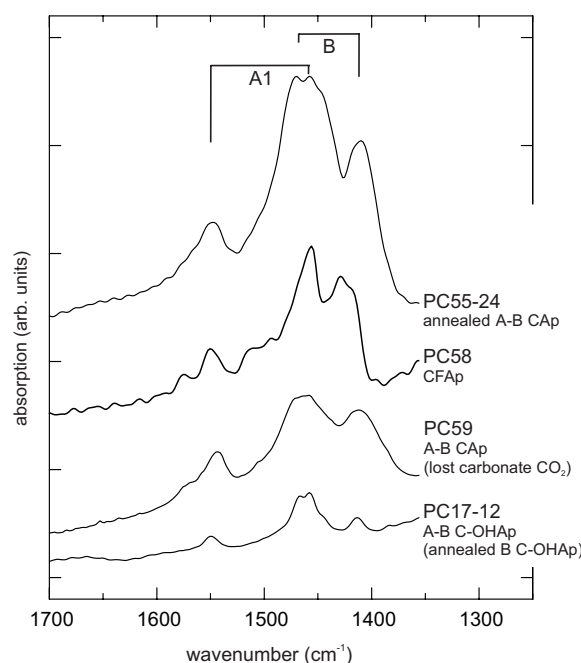


**FIGURE 4.** FTIR spectrum of carbonated FAp (CFAp; PC58) compared with spectra for type A-B CAP annealed in air at 1000 °C for 24 hours (PC55-24) and an experiment that appeared to have lost carbonate CO<sub>2</sub> (PC59), and type B C-OHAp annealed in air at 1000 °C for 12 hours to give type A-B C-OHAp (PC17-12); bands of asymmetric stretching ( $\nu_3$ ) doublets for type B and A1 carbonate ion are indicated.

of the bands of the type B doublet, due to overlap of the low-frequency band with that for calcite and of the high-frequency band with the low-frequency band of the type A1 doublet. The former interference can be eliminated by thermal decarbonation of the

calcite. The spectrum for PC55 annealed in air at 1000 °C for 24 hours (Fleet and Liu 2004) is reproduced in Figure 4 (PC55-24). Although some compositional and structural changes also occur concomitantly in the CAP, comparison of the high-pressure and annealed products (Figs. 2 and 4, respectively) clearly indicates that the prominence of the  $\sim 1406\text{ cm}^{-1}$  band in the piston-cylinder product is due to admixed calcite. The second type of interference, overlap of the high-frequency band of the type B doublet with the low-frequency band of the type A1 doublet, is more troublesome, and a case could be made for reversing the present assignments of these two peaks. Indeed, review of the literature showed that precise IR peak positions for the carbonate ion in apatite do vary, in some cases significantly (Regnier et al. 1994). Nevertheless, most literature studies have assigned the higher-frequency band (or shoulder) to the type B carbonate ion, and this assignment optimized the correspondence between the fitted peak areas and X-ray structural analysis site occupancies, in both Fleet and Liu (2004) and the present study.

From Table 1 and Figures 2–5, molar  $1/3(\text{Ca}_2\text{P}_2\text{O}_7 + \text{CaO}) : \text{CaCO}_3 = 9:1$  yields either type A CAP or type A C-OHAp. Experiment PC56 duplicates PC71 and shows that the results of Fleet and Liu (2003) are readily reproducible. Our earlier experiments on apatite synthesis using the piston-cylinder apparatus evidently did not exclude all sources of contamination by water (or hydrogen). In addition, based on the low yields of carbonate,

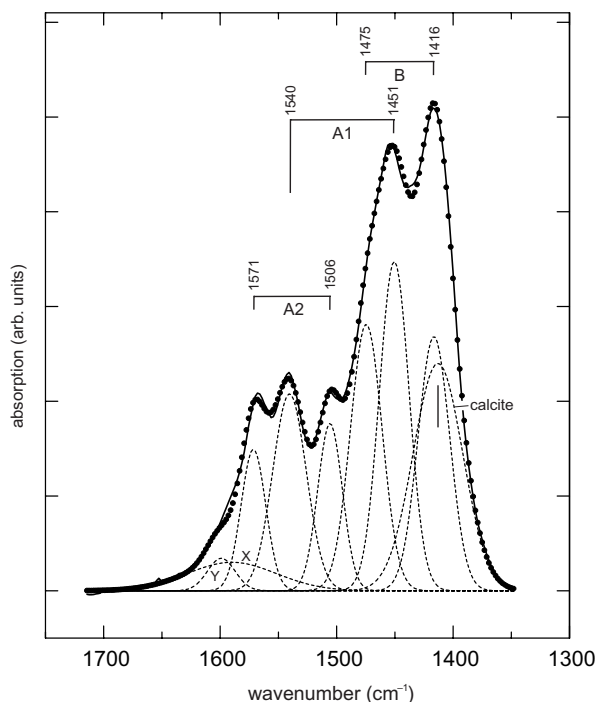


**FIGURE 5.** FTIR spectrum of type A-B CAP synthesized at 3 GPa (PC18) fitted with Gaussian distributions for bands due to asymmetric stretching ( $\nu_3$ ) of type B, A1, and A2 carbonate ions and calcite: X and Y are Gaussian peaks added to facilitate convergence of least-squares refinement, and represent complexity in the high-frequency region of the spectrum (cf., LeGeros et al. 1969; Nelson and Featherstone 1982; Regnier et al. 1994; Suetsuga et al. 1998; Vignoles et al. 1988; Comodi and Liu 2000); dots show fitted envelope (see Table 7).

containment of carbonate  $\text{CO}_2$  may not have been successful both in the preparation of starting materials and during high-pressure reaction. Thus, PC16 and PC17 resulted in C-OHAp, close in composition to end-member OHAp (Fig. 2), rather than CAP; PC16, in particular, is a type A C-OHAp (Fig. 3), with minor A2 and a trace of B carbonate. Most experiments with molar  $1/3(\text{Ca}_2\text{P}_2\text{O}_7 + \text{CaO}) : \text{CaCO}_3 = 8:2$  yielded type A-B CAP with minor calcite, present as dispersed, admixed grains. The FTIR spectra of PC55 and PC73 are very similar and indicate, from low to high wavenumber, significant contents of calcite, type B and type A1 carbonate and a subordinate content of type A2 carbonate. On the other hand, the *c*-axis channel of PC17 apatite is very largely blocked to carbonate by  $\text{OH}^-$ . This C-OHAp phase has a low total carbonate content, with an FTIR spectrum dominated by type B carbonate and only subordinate type A1 and A2 carbonate. Experiment PC17 was clearly contaminated by water and lost carbonate  $\text{CO}_2$ , but the relatively low phosphate content and high  $\text{CaO} : \text{P}_2\text{O}_5$  ratio in the starting composition ensured that the resulting C-OHAp (Fig. 3) was dominantly of type B. Carbonate-rich melt was encountered in all experiments with a higher proportion of  $\text{CaCO}_3$  and quenched from high temperature (PC18, PC57, PC59, and PC26). The pronounced enhancement of the FTIR absorption at  $1400\text{--}1475\text{ cm}^{-1}$  appears to reflect a greater proportion of calcite, rather than of type B carbonate ion (cf., PC18 and PC57 in Fig. 2). This conclusion is supported by the present X-ray studies on crystals from PC18. Note that PC53, which was annealed at 1000 °C at high pressure, shows diminution in the strength of high-frequency bands, similarly to that reported for PC55 annealed at room pressure in Fleet and Liu (2004), but attributable, in this case, to blocking of channel sites to carbonate by a high content of  $\text{OH}^-$ .

The FTIR spectrum for a single experiment on the synthesis of carbonated FAp (CFAP; PC58) is compared in Figure 4 with those for samples of PC55 (A-B CAP) and PC17 (B C-OHAp) annealed in air and for an experiment at 3 GPa, 1500 °C made with molar  $1/3(\text{Ca}_2\text{P}_2\text{O}_7 + \text{CaO}) : \text{CaCO}_3 = 7:3$  that appeared to have lost carbonate  $\text{CO}_2$  after initial crystallization of CAP (PC59). Evidently, the centroid of the type B doublet in the spectrum for CFAP more-or-less corresponds with that of the type B doublet in type A-B CAP and type B C-OHAp but the peak splitting is diminished, so that the high-frequency band aligns with the presently assigned low-frequency band of the type A1 doublets. Thus, CFAP does not appear to be a suitable labeled compound for the type B carbonate ion in CAP and C-OHAp (cf., Regnier et al. 1994). Another interesting feature displayed by Figure 4 is the similarity in the FTIR spectra of annealed CAP (PC55) and C-OHAp (PC17-12). Fleet and Liu (2004) noted that annealing of PC55 products resulted in loss of type A2 carbonate (and dehydroxylation) and some reorganization of the remaining carbonate; compared with the unannealed product, the spectrum of PC17-12 shows the emergence of a well-organized type A1 carbonate ion component.

Three of the new experiments (Fig. 3) were supported by X-ray structural analysis on single-crystal products and, for one of these (PC18), the spectral region for asymmetric stretching of the carbonate ion has been peak fitted with Gaussian distributions using the programme BGAUSS (Tyliszczak 1992; present Fig. 5). Additional Gaussian peaks at  $1590$  and  $1599\text{ cm}^{-1}$  were

introduced to model the poorly fitted high-frequency features. Convergence of the least-squares refinement was achieved by fixing band widths for the apatite carbonate ions, as well as all parameters for the calcite singlet band (at 1413  $\text{cm}^{-1}$ ) and the Gaussian peaks at 1590 and 1599  $\text{cm}^{-1}$  (Table 7). As detailed in Fleet and Liu (2004), interpretation of the spectral features is at best semi-quantitative due to the complex nature of the spectra, limitations in the fitting model and fitting procedure of the program BGAUSS, and inadequate background correction. The  $\nu_3$  region of the infrared spectrum of CAp of complex composition typically has a saw-tooth profile, in both this and literature studies, rising abruptly from the background on the low-frequency side and fading into the background on the high-frequency side. In particular, the spectrum of the type A2 carbonate is certainly more complicated than that presently represented, and the contribution of this (type A2) carbonate species is underestimated in the present fitting procedure. The peak widths in Table 7 and Figure 5 were assigned to optimize the fit, and differences between limbs of the same doublet are of unknown significance. We also recognize that variation of the molecular extinction coefficient for carbonate (and hydroxyl) ions with local stereochemical environment may invalidate the precise correspondence between FTIR peak area and site occupancy. Fitting of the FTIR spectra of PC16 and PC17 was not attempted because many of the features of interest were only weakly present above background. Finally, change in the band for the out-of-plane bending vibration ( $\nu_2$ ) at  $\sim 875 \text{ cm}^{-1}$  has not been documented. This band was clearly complex for complex type A-B CAp (e.g., PC18 in Fig. 3; cf., Regnier et al. 1994), but the resolution of spectral features was inferior to that of the asymmetric stretching ( $\nu_3$ ) region.

### X-ray structural analysis

The crystal structures of PC17, PC16, and two crystals of PC18 were refined by single-crystal XRD analysis (Tables 2–5). Crystal xt371 from PC18 had been stored in nujol oil for four months, and room-temperature contamination by water was suspected. Therefore, study of PC18 was supported by

investigation of a second crystal (xt373) stored dry in a desiccated glass vial. Structure refinement for the two crystals from PC18 closely followed that for PC55 in Fleet and Liu (2004), and resulted in similar structures, albeit with somewhat lower contents of carbonate in the new structures; the total carbonate contents being 1.37, 1.57 and 1.84 pfu for xt371, xt373 and PC55, respectively. Although the site occupancies (Table 4) used in the calculation of carbonate ion contents are only marginally lower for xt371 than xt373, it appears that PC18 may have lost some of its channel carbonate through exchange with  $\text{OH}^-$  during room-temperature storage in nujol oil exposed to laboratory air. The X-ray structural refinements showed a deficiency of electron density at P and O3 (indicating partial replacement of phosphate by type B carbonate; Wilson et al. 1999), and weak electron density at the positions OH (interpreted as a combination of minor  $\text{OH}^-$  or  $\text{O}^{2-}$ , and one oxygen atom of the type A2 carbonate ion), OA2 (interpreted as the other two oxygen atoms of the type A2 carbonate ion), C (at the origin), OA11 and OA12 (interpreted as the three oxygen atoms of the type A1 carbonate ion; the two oxygen atoms close to the *c*-axis are essentially coincident in the average structure and are reported as OA11), and OB3 (one oxygen of the type B carbonate ion). As noted earlier, all of the carbonate oxygen atoms are in general positions and disordered with a multiplicity of twelve. Because of their extensive overlap and very weak electron density contributions, it was not possible to refine simultaneously both occupancy and displacement parameters for atoms of the carbonate ions. Instead, an arbitrary isotropic displacement (thermal) parameter of value  $U = 0.025 \text{ \AA}^2$  was assigned to each of these atoms and the refinement was allowed to converge by varying the site occupancies. In addition, the occupancy of O3 was constrained to  $[1.0 - (0.5 - P)]$ . The refined O-O distances for the three carbonate ions in xt373 are: 2.22, 2.12, and 1.90  $\text{\AA}$  for type A1; 2.15, 1.77, and 1.71  $\text{\AA}$  for type A2; and 2.44, 2.51, and 2.09  $\text{\AA}$  for type B. The results for the type A1 carbonate ion are similar to those obtained for PC55 (Fleet and Liu 2004) and in reasonable agreement with the expected O-O distance (e.g., 2.219  $\text{\AA}$  in calcite; Smyth and Bish 1988). The short O-O distances found for the type A2 carbonate ion reflect the smaller amount of A2 carbonate present in xt373 (Table 7) and the high correlation between OA12 and OA2, which are in close proximity in the average structure. The type B carbonate ion is not well defined due to overlap with O1 and O2 in the average structure.

The formula amounts of the three structurally distinct carbonate ions are compared with the amounts derived from the corresponding FTIR spectra in Table 7: note that the formula amount of type A1 carbonate is the *x* compositional variable and that of type B is *y* of the schematic formula (3). The electron density of OA12 was used to estimate the formula amount of type A1 carbonate in both Tables 2 and 7, because this atom is better resolved than OA11 and free of assumptions used to refine the overlapped electron density for atoms close to the *c*-axis. The electron density of OB3 was used for type B carbonate, and one-half of that of OA2 for type A2 carbonate. All carbonate oxygen atoms are disordered with a multiplicity of 12 and, in addition, the electron density at OA2 represents two non-equivalent oxygen atoms superimposed in the average CAp structure. Thus, using the site occupancy data in Table 4, the *y* compositional variable

**TABLE 7.** Fitted FTIR spectra and formula amounts of carbonate for type A-B CAp

Band	PC18			PC55‡			
	fitted FTIR spectra			Position	Width*	Peak	
	Position	Width*	Peak	Position	Width*	Peak	
	$\text{cm}^{-1}$	$\text{cm}^{-1}$	area†	$\text{cm}^{-1}$	$\text{cm}^{-1}$	area	
Type A1 doublet	1451	30	11.1	1449	32	7.3	
	1540	34	7.5	1540	30	7.5	
Type A2 doublet	1506	25	4.7	1507	28	4.6	
	1571	25	4.0	1569	32	6.2	
Type B doublet	1416	32	9.1	1408	32	6.7	
	1475	32	9.6	1474	30	6.3	
Calcite*	1413	50	12.8	1409	56	8.9	
Formula amounts of carbonate§							
	xt371		xt373			xt376	
Carbonate ion type	A1	A2	B	A1	A2	B	
FTIR spectra	(0.59)	0.25	0.49	(0.69)	0.29	0.56	
X-ray structure	0.59	0.37	0.41	0.69	0.39	0.49	
				0.69	0.57	0.57	

\* Not refined.

† Relative values.

‡ Fleet and Liu (2004).

§ See Table 2 footnote for formulae, and text for calculation procedures.

|| (0.59) dependent value.

for PC17 (type B C-OHAp; Table 2) is  $0.014 \times 12 \approx 0.17$ , and the formula amount of type A2 carbonate in PC18, crystal xt371 (type A-B CAP; Table 7) is  $(0.062 \times 12)/2 \approx 0.37$ . The refined occupancy of O4 was not used to estimate formula amounts of OH, due to the extensive overlap of the hydroxyl oxygen and apical oxygen of the type A2 carbonate ion along the *c*-axis of the average structures. In addition, the refined values of 0.72(5) and 0.65(6) for H of PC17 and PC16, respectively, in Table 4 merely demonstrate that the adopted fixed values for the *z* atomic coordinate and the thermal parameter *U* were reasonable. In the  $P6_3/m$  structure of OHAp (Hughes et al. 1989), the OH<sup>-</sup> ion is disordered with a multiplicity of 4, so that, for two OH pfu, H has an occupancy of 0.5. The formula amounts of type B and A2 carbonate from FTIR spectroscopy were calculated by equating the peak area of the low-frequency band of the type A1 doublet with the type A1 carbonate occupancy of the corresponding X-ray structural analysis.

The structures of PC17 and PC16 are very similar to that of end-member OHAp (e.g., Hughes et al. 1989; Fleet and Pan 2000a). The hydrogen atom was clearly resolved but, different from Fleet and Pan (2000a), the H-O distance was constrained ( $\sim 1.0$  Å) to permit refinement of the H site occupancy. PC17 was refined for type B carbonate and PC16 for type A1 carbonate, based on the dominant carbonate ion contribution to their FTIR spectra (Figs. 2 and 3). Maximum and minimum residual electron densities were located near Ca2 in all four structures.

The results of the various single-crystal XRD measurements on CAP and C-OHAp synthesized at high-pressure are summarized in Table 2. Type A CAP with  $x \geq 0.5$  and  $y = 0.0$  crystallizes with a partially ordered structure in space group  $P\bar{3}$ . All other compositions investigated in our studies (including type B C-OHAp with  $y \approx 0.17$ , type A C-OHAp with  $x \approx 0.14$ , and type A-B CAP with  $x \geq 0.6$  and  $y \geq 0.4$ ) crystallized with average structures in space group  $P6_3/m$ . In addition, annealed crystals of PC55 showed significant intensity for 003 (Fleet and Liu 2004), which is by far the strongest reflection defining the lower symmetry ( $P\bar{3}$ ) space group, although the intensity of  $hkl, h\bar{k}l$  reflection pairs remained identical within error of measurement. These results are readily understood from consideration of the  $P\bar{3}$  structure (Fleet and Liu 2003), which requires ordering of the type A1 carbonate ions within the apatite channel, because a disordered distribution results in prohibitively close O-O distances for some neighbouring carbonate ions. The need for ordering is relaxed when the type A1 carbonate ions are interspersed with OH<sup>-</sup> and type A2 carbonate ions are in the stuffed channel position, as shown in Fleet and Liu (2004), as well as by the greater disruption of the overall apatite structure resulting from the introduction of type B carbonate. Thus, when samples are annealed, reorganization results in diffraction-sized crystallite domains of locally ordered structure. The seemingly disordered structures of the pressure-quenched CAP and C-OHAp may be composite structures as well, and formed complexly of mixed domains in twin orientation. Note that O4, which represents contributions from the type A2 carbonate and hydroxyl ions in the structure of xt373 (Tables 4 and 5), has an off-axis location, showing that the crystal space group  $P6_3/m$  more probably represents a composite averaged structure than one randomly disordered at the atomic level. CAP and C-OHAp of bone and dental enamel may also

have composite structures, but this aspect is beyond the scope of the present study.

We suggest that the apatites of Fleet and Liu (2003, 2004) and this study do properly represent the structural features of low-temperature natural and precipitated CAP and C-OHAp, and of bioapatites as well, even though the crystals investigated were synthesized at 2–4 GPa. However, the entry of moderate amounts of carbonate ion into the stuffed A2 channel location does appear to be a high-pressure feature, as bands attributable to type A2 carbonate are only weakly present in IR spectra of low-pressure CAP, as a sharp peak or shoulder at  $\sim 1500$  cm<sup>-1</sup> and diffuse absorption at higher frequency (Nelson and Featherstone 1982; Vignoles et al. 1988; Barralet et al. 1998; Suetsugu et al. 1998). Therefore, charge compensation for carbonate-for-phosphate substitution in low-pressure CAP is different from that in high-pressure CAP (equation 2), and likely involves nonstoichiometry in Ca positions, as well as partial substitution of Ca by Na, in bone and enamel. In contrast, our X-ray structural studies suggested that Ca1 and Ca2 positions were fully occupied in high-pressure CAP.

As reviewed above, Suetsugu et al. (2000) and Ivanova et al. (2001) deduced locations for type A1 and B carbonate, respectively, that are different from those suggested by our studies (Fleet and Liu 2003, 2004; this study). It is possible that the structures of other preparations of C-OHAp and CAP are more complicated than presently proposed. However, the  $\nu_3$  infrared spectrum for type A-B CAP in Suetsugu et al. (1998) and Raman data for type B C-OHAp in Ivanova et al. (2001) are consistent with this and other literature studies, and it seems unlikely that different stereochemical environments would result in essentially the same vibrational spectrum for any given type of carbonate ion. Clearly, these inter-laboratory uncertainties in structural details do require further study. The presently assumed location for type A1 carbonate is well established by the  $P\bar{3}$  structure of Fleet and Liu (2003). Suetsugu et al. (1998, 2000) apparently did not investigate the possibility that their crystal symmetry might be twinned  $P\bar{3}$  and we note that their thermal parameters for the off-axis carbonate O atoms are too large for meaningful (constrained) refinement of the type A1 carbonate ion. The Ivanova et al. (2001) structure was determined by Rietveld refinement of powder XRD data; given that the apatite grain size was about 10  $\mu$ m, it should be possible to reinvestigate this material by single-crystal synchrotron crystallography.

The response of the unit-cell parameters of apatite to accommodation of the carbonate ion is complex. Substitution of OH<sup>-</sup> by type A carbonate results in progressive increase in *a* and decrease in *c* (LeGeros et al. 1969; Bonel 1972), whereas substitution of phosphate by type B carbonate results in progressive decrease in *a* and increase in *c* (Nelson and Featherstone 1982; Vignoles et al. 1988). Thus, compared with the type A calibration curve of Bonel (1972), *a* and *c* are close to end-member OHAp for PC17 [cf., *a* = 9.4202(8) and *c* = 6.8832(5) Å for Sm-substituted OHAp in Fleet and Pan 2000a], correspond to C-OHAp with about twice as much carbonate as presently found for PC16, and are in good agreement with the higher contents of carbonate determined for PC74 and PC71. Also, the unit-cell parameters of the annealed samples are in fair agreement with those for type A-B CAP synthesized at 0.55 kbar (Suetsugu et al. 1998, 2000).

### Accommodation of carbonate by OHAp

The accommodation of the carbonate ion in the *c*-axis channel of hydroxylapatite is not a straightforward atom-for-atom substitution. Compared with OH<sup>-</sup>, carbonate is a bulky divalent anion (essentially a cluster of three non-bonded oxygen atoms replacing one), so that its accommodation in OHAp requires both displacement of atoms in the channel wall and redistribution of Ca-O bonds. The type B carbonate ion is seemingly accommodated more readily, but still requires displacement of the second O3 atom away from the bonding sphere of the carbonate ion and extension of the overall structure in the *c*-axis direction. The anisotropic displacement ellipsoids of the present synthetic apatites reflect the relative displacement of the constituent atoms because their crystal structures are an average of all possible combinations of locally ordered structure of lower symmetry and, thus, provide an important window into the structural adjustments required to accommodate the carbonate ion.

When a carbonate ion of ideal geometry is inserted into the channel of OHAp with the apical oxygen atom coincident with the position of OH, as in Figure 1a, it is evident that the other two (transverse) carbonate oxygen atoms interact unfavorably with the tricluster of Ca<sub>2</sub> cations at  $z = -0.25$ . In the limiting orientation of Figure 1a, one of these oxygen atoms makes a short (1.65 Å) bond with a Ca<sub>2</sub> atom and a short (2.17 Å) non-bonded O···O interaction with O3 of the nearby PO<sub>4</sub> tetrahedron. Clearly, the carbonate ion has to be twisted about the *c*-axis to optimize Ca-O and O-O distances, but this still leaves unacceptably short interactions in the absence of other displacements.

Although the atoms of the carbonate ion in the  $P\bar{3}$  structure of type A CAp are disordered, ordering of the carbonate along the apatite channel at  $z = 0.5$  permitted a ready and fairly precise reconstruction of the configuration of the type A1 carbonate ion and gave unique insight into the nature of the atomic displacements of the intermediate-range structure (Fleet and Liu 2003). The type A1 carbonate ion is oriented with two of its oxygen atoms (OA11) close to the *c*-axis and its plane canted from the vertical by  $\sim 12^\circ$ . It is located in the apatite channel by six bonds to Ca<sub>2</sub> atoms, giving Ca<sub>2</sub>-O bond distances consistent with an ideal distribution of valence units for the carbonate ion oxygen atoms (i.e., 4/3 to C and 1/3 to 2 × Ca<sub>2</sub>). However, for the ideal geometry of the OHAp host structure (space group  $P6_3/m$ ; Fig. 1b), the third oxygen atom (OA12) interacts closely (2.06 Å) with O3 of the nearby PO<sub>4</sub> tetrahedron, requiring rotation and rigid body displacement of the tetrahedron. Overall, the phosphate groups are displaced slightly from ideal OHAp positions to dilate the apatite channel in the immediate vicinity of the carbonate ion, and to contract it above and below (i.e., at  $z \pm 0.5$ ). These adjustments are most evident in the complementary change in the coordination of Ca1 in the  $P\bar{3}$  structure. In the  $P6_3/m$  structure of OHAp and FAp, Ca1 has nine nearest-neighbor oxygen atoms in the configuration of a tricapped trigonal prism, which also can be regarded as 6+3 coordination (Fleet et al. 2000b). Although Ca1A is in a stretched ninefold coordination at  $z \approx 0.0$  in the  $P\bar{3}$  structure, Ca1B, at  $z \approx 0.5$ , is in a compact sixfold trigonal prismatic coordination, which compensates dilation of the apatite channel at the same structural height.

The type A2 carbonate ion is represented by two “transverse” OA2 atoms, which are approximately related by inversion

through the origin, and an apical oxygen atom at the height of a tricluster of Ca<sub>2</sub> cations (at  $z = -0.25$  in Fig. 1c). The type A2 carbonate is then in an open vertical configuration but rotated about a horizontal axis and tilted slightly away from the *c*-axis (Fig. 1c). As depicted in Figure 1c, it is smaller than ideal carbonate ion geometry due to the difficulties in resolving the constituent atoms in the type A-B CAp structures of PC55 and PC18 (Fleet and Liu 2004; this study). Nevertheless, the OA2 oxygen atom bonded to two Ca<sub>2</sub> atoms at  $z = 0.25$  has a close (2.05 Å) interaction with an O3 oxygen atom of the nearby PO<sub>4</sub> tetrahedron, requiring further structural adjustments.

The progressive increase in the *a* unit-cell edge length with increase in carbonate content of type A CAp (LeGeros et al. 1969; Bonel 1972) is readily attributed to the dilation of the apatite channel required to accommodate the type A1 carbonate. Accommodation of the type A2 carbonate ion should have a similar effect but, because A2 carbonate tends to be present with and in subordinate amounts to type B carbonate, its effect on the unit-cell parameters is overwhelmed by the expansion of *c* (and contraction of *a*; Nelson and Featherstone 1982; Vignoles et al. 1988) in response to displacement of O3 along  $\pm[001]$  to accommodate the type B carbonate ion.

The atomic displacement parameters for the synthetic apatites of Fleet and Liu (2003, 2004, this study) increase progressively with increase in total carbonate content, as expected, but this increase is differential from one structural position to another and from one parameter to another for the same position and appears to be greater for type A carbonate than for type B (Fig. 6). The reference OHAp structure used in Figure 6 is that of a synthetic Sm-substituted apatite from Fleet et al. (2000a). The displacement parameters of Ca<sub>2</sub>, O<sub>2</sub>, and O<sub>3</sub> show the greatest change with variation in carbonate content, with  $U_{\text{eq}}$  increasing by about 2.5× over the range in total apatite carbonate investigated, compared with 1.5× for Ca<sub>1</sub> and O<sub>1</sub>. Moreover, the anisotropy of the displacement ellipsoids of O<sub>2</sub> and O<sub>3</sub> becomes more exag-

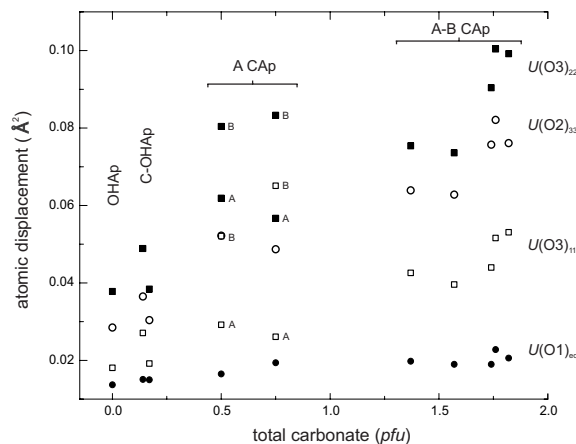


**FIGURE 6.** Progressive increase in selected atomic displacement parameters of apatite with increase in total carbonate ion content: filled circles are  $U(O1)_{\text{eq}}$ , the equivalent isotropic displacement of O1; open circles are  $U(O2)_{33}$ ; open squares are  $U(O3)_{11}$ ; and filled squares are  $U(O3)_{22}$ ; note that in the  $P\bar{3}$  structure of type A CAp there are two non-equivalent O3 oxygen atoms (labeled A and B) with quite different stereochemical environments.

gerated from type A or B C-OHAp to type A CAp and type A-B CAp, with  $U_{33} \gg (U_{11}, U_{22})$  for O2 and  $U_{22} > U_{11} > U_{33}$  for O3. The two views of the displacement ellipsoids for the PO<sub>4</sub> tetrahedron of type B C-OHAp from PC17, type A CAp from PC71, and type A-B CAp from PC55 in Figure 7 are clearly consistent with rotation of the tetrahedron about the P-O1 bond. This rotation shifts O3 away from its short interaction with OA12 of type A1 carbonate (Fig. 1b) and OA2 of type A2 carbonate (Fig. 1c). Therefore, we conclude that accommodation of the carbonate ion in the *c*-axis channel of OHAp is affected, complexly, by dilation of the apatite channel, contraction of the Ca1O<sub>n</sub> polyhedron, and simple rotation of the PO<sub>4</sub> tetrahedron in the vicinity of the carbonate ion. Displacements due to accommodation of the type B carbonate ion alone are not evident in the present structures, because we did not succeed in preparing CAp dominated by type B. Also, we have not attempted to analyze the complex displacements of Ca2 in the average structures. It is obvious that Ca2 has to be displaced locally to optimize Ca2-O bond strengths. These complex shifts in the position of Ca2 are reflected in its anomalously large displacement ellipsoid and association with the maximum and minimum residual electron density in all of the carbonated and carbonate apatites investigated by us.

#### ACKNOWLEDGMENTS

We thank J. Hughes, K. Rogers, and one anonymous reviewer for helpful comments, M. Jennings for collection of the X-ray reflection data, R. Tucker for

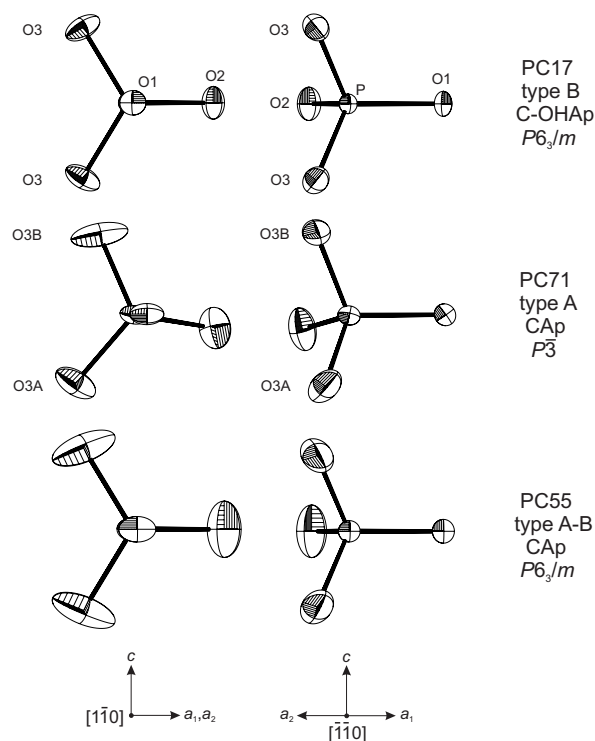


**FIGURE 7.** Two views of the PO<sub>4</sub> tetrahedron showing anisotropic displacement of O2 and O3 atoms in three synthetic apatite samples, reflecting increase in displacement of tetrahedron about P-O1 axis with increase in carbonate ion content: drawn with ATOMS (Dowty 1995).

assistance with preparation of the piston-cylinder assemblies and apparatus, and the Natural Sciences and Engineering Research Council of Canada for financial support (M.E.F., P.L.K.). The Canada Foundation for Innovation provided funding for the FTIR spectrometer (P.L.K.).

#### REFERENCES CITED

- Barralet, J., Best, S., and Bonfield, W. (1998) Carbonate substitution in precipitated hydroxyapatite: An investigation into the effects of reaction temperature and bicarbonate ion concentration. *Journal of Biomedical Materials Research*, 41, 79–86.
- Beshah, K., Rey, C., Glimcher, M.J., Schimizu, M., and Griffin, R.G. (1990) Solid state carbon-13 and proton NMR studies of carbonate-containing calcium phosphates and enamel. *Journal of Solid State Chemistry*, 84, 71–81.
- Bohlen, S.R. (1984) Equilibria for precise pressure calibration and a frictionless furnace assembly for the piston-cylinder apparatus. *Neues Jahrbuch Mineralogie, Monatshefte*, 9, 404–412.
- Bohlen, S.R. and Boettcher, A.L. (1982) The quartz ↔ coesite transformation: a precise determination and the effects of other components. *Journal of Geophysical Research*, 87, 7073–7078.
- Bonel, G. (1972) Contribution à l'étude de la carbonatation des apatites. I. Synthèse et étude des propriétés physico-chimiques des apatites carbonatées du type A. *Annales de Chimie (Paris, France)*, 7, 65–88.
- Comodi, P. and Liu, Y. (2000) CO<sub>3</sub> substitution in apatite: further insight from new crystal-chemical data of Kasekere (Uganda) apatite. *European Journal of Mineralogy*, 12, 965–974.
- Coppens, P. (1977) *LINEX77*. State University of New York, Buffalo.
- Dorozhkin, S.V. and Epple, M. (2002) Biological and medical significance of calcium phosphates. *Angewandte Chemie International Edition*, 41, 3130–3146.
- Dowker, S.E.P., Anderson, P., Elliott, J.C. and Gao, X.J. (1999) Crystal chemistry and dissolution of calcium phosphate in dental enamel. *Mineralogical Magazine*, 63, 791–800.
- Dowty, E. (1995) *ATOMS for Windows*. Version 3.1. Shape Software, 521 Hidden Valley Road, Kingsport, TN 37663, USA.
- Elliott, J.C. (1964) The interpretation of the infra-red absorption spectra of some carbonate-containing apatites. In R.W. Fearnhead and M.V. Stack, Eds., *Tooth Enamel: Its composition, properties, and fundamental structure*, pp. 20–22. John Wright & Sons, Bristol, U.K.
- (1994) *Structure and Chemistry of the Apatites and Other Calcium Orthophosphates*. Elsevier, Amsterdam.
- (1998) Recent studies of apatites and other calcium orthophosphates. In: *Les matériaux en phosphate de calcium. Aspects fondamentaux*, E. Brès and P. Hardouin, Eds., Sauramps Medical, Montpellier, 25–66.
- (2002) Calcium phosphate biominerals. In M.J. Kohn, J. Rakovan and J.M. Hughes, Eds., *Phosphates*, pp. 427–453. Reviews in Mineralogy and Geochemistry, 48, Mineralogical Society of America, Washington, D.C.
- Elliott, J.C., Bonel, G., and Trombe, J.C. (1980) Space group and lattice constants of Ca<sub>10</sub>(PO<sub>4</sub>)<sub>6</sub>CO<sub>3</sub>. *Journal of Applied Crystallography*, 13, 618–621.
- Fleet, M.E. and Liu, X. (2003) Carbonate apatite type A synthesized at high pressure: new space group (*P*<sup>3</sup>) and orientation of channel carbonate ion. *Journal of Solid State Chemistry*, 174, 412–417.
- (2004) Location of type B carbonate ion in type A-B carbonate apatite synthesized at high pressure. *Journal of Solid State Chemistry*, in press.
- Fleet, M.E. and Pan, Y. (1995) Site preference of rare earth elements in fluorapatite. *American Mineralogist*, 80, 329–335.
- (1997) Site preference of rare earth elements in fluorapatite: Binary (LREE+HREE)-substituted crystals. *American Mineralogist*, 82, 870–877.
- Fleet, M.E., Liu, X., and Pan, Y. (2000a) Site preference of rare earth elements in hydroxyapatite [Ca<sub>10</sub>(PO<sub>4</sub>)<sub>6</sub>(OH)<sub>2</sub>]. *Journal of Solid State Chemistry*, 149, 391–398.
- (2000b) Rare earth elements in chlorapatite [Ca<sub>10</sub>(PO<sub>4</sub>)<sub>6</sub>(Cl)<sub>2</sub>]: Uptake, site preference and degradation of monoclinic structure. *American Mineralogist*, 85, 1437–1446.
- Gross, K.A. and Berndt, C.C. (2002) Biomedical application of apatites. In M.J. Kohn, J. Rakovan and J.M. Hughes, Eds., *Phosphates*, pp. 631–672. Reviews in Mineralogy and Geochemistry, 48, Mineralogical Society of America, Washington, D.C.
- Gunawardane, R.P., Howie, R.A., and Glasser, F.P. (1982) Structure of the oxyapatite NaY<sub>9</sub>(SiO<sub>4</sub>)<sub>6</sub>O<sub>2</sub>. *Acta Crystallographica*, B38, 1564–1566.
- Hughes, J.M. and Rakovan, J. (2002) The crystal structure of apatite, Ca<sub>5</sub>(PO<sub>4</sub>)<sub>3</sub>(F,OH,Cl). In M.J. Kohn, J. Rakovan and J.M. Hughes, Eds., *Phosphates*, pp. 1–12. Reviews in Mineralogy and Geochemistry, 48, Mineralogical Society of America, Washington, D.C.
- Hughes, J.M., Cameron, M., and Crowley, K.D. (1989) Structural variations in natural F, OH, and Cl apatites. *American Mineralogist*, 74, 870–876.
- Ibers, J.A. and Hamilton, W.C. Eds. (1974) *International Tables for X-ray Crystallography*, Vol. IV. Kynoch Press, Birmingham, UK.
- Ivanova, T.I., Frank-Kamenetskaya, O.V., Kol'tsov, A.B., and Ugol'kov, V.L. (2001) Crystal structure of calcium-deficient carbonated hydroxyapatite. Thermal decomposition. *Journal of Solid State Chemistry*, 160, 340–349.

- LeGeros, R.Z., Trautz, O.R., Klein, E., and LeGeros, J.P. (1969) Two types of carbonate substitution in the apatite structure. *Experientia* 25, 5–7.
- Mackie, P.E. and Young, R.A. (1973) Location of Nd dopant in fluorapatite,  $\text{Ca}_5(\text{PO}_4)_3\text{F:Nd}$ . *Journal of Applied Crystallography*, 6, 26–31.
- Mackie, P.E., Elliott, J.C., and Young, R.A. (1972) Monoclinic structure of synthetic  $\text{Ca}_5(\text{PO}_4)_3\text{Cl}$ , chlorapatite. *Acta Crystallographica*, B 28, 1840–1848.
- Nelson, D.G.A. and Featherstone, J.D.B. (1982) Preparation, analysis, and characterization of carbonated apatites. *Calcified Tissue International*, 34, S69–S81.
- Nonius (1997) COLLECT Software. Nonius, Delft, The Netherlands.
- Pan, Y. and Fleet, M.E. (2002) Compositions of the apatite-group minerals: substitution mechanisms and controlling factors. In M.J. Kohn, J. Rakovan and J.M. Hughes, Eds., *Phosphates*, pp. 13–49. *Reviews in Mineralogy and Geochemistry*, 48, Mineralogical Society of America, Washington, D.C.
- Penel, G., Leroy, G., Rey, C., and Bres, E. (1998) MicroRaman spectral study of the  $\text{PO}_4$  and  $\text{CO}_3$  vibrational modes in synthetic and biological apatites. *Calcified Tissue International*, 63, 475–481.
- Piccoli, P.M. and Candela, P.A. (2002) Apatite in igneous systems. In M.J. Kohn, J. Rakovan, and J.M. Hughes, Eds., *Phosphates*, pp. 255–292. *Reviews in Mineralogy and Geochemistry*, 48, Mineralogical Society of America, Washington, D.C.
- Regnier, P., Lasaga, A.C., Berner, R.A., Han, O.H., and Zilm, K.W. (1994) Mechanism of  $\text{CO}_3^{2-}$  substitution in carbonate-fluorapatite: Evidence from FTIR spectroscopy,  $^{13}\text{C}$  NMR, and quantum mechanical calculations. *American Mineralogist*, 79, 809–818.
- Siemens (1993) SHELXTL PC (Version 4.1). Siemens Analytical X-ray Instruments, Inc., Madison, WI 53719, U.S.A.
- Smyth, J.R. and Bish, D.L. (1988) *Crystal Structures and Cation Sites of the Rock-Forming Minerals*. Allen & Unwin, London.
- Suchanek, W.L., Shuk, P., Byrappa, K., Riman, R.E., TenHuisen, K.S., and Janas, V.F. (2002) Mechanochemical-hydrothermal synthesis of carbonated apatite powders at room temperature. *Biomaterials*, 23, 699–710.
- Suetsugu, Y., Shimoya, I., and Tanaka, J. (1998) Configuration of carbonate ions in apatite structure determined by polarized infrared spectroscopy. *Journal of the American Ceramic Society*, 81, 746–748.
- Suetsugu, Y., Takahashi, Y., Okamura, F.P., and Tanaka, J. (2000) Structure analysis of A-type carbonate apatite by a single-crystal X-ray diffraction method. *Journal of Solid State Chemistry*, 155, 292–297.
- Tyliszczak, T. (1992) BAN Data Analysis Program, McMaster University.
- Vignoles, M., Bonel, G., Holcomb, D.W., and Young, R.A. (1988) Influence of preparation conditions on the composition of type B carbonated hydroxyapatite and on the localization of the carbonate ions. *Calcified Tissue International*, 43, 33–40.
- White, W.B. (1974) The carbonate minerals. In V.C. Farmer, Ed., *The Infrared Spectra of Minerals*, Monograph 4, pp. 227–284. Mineralogical Society of London, U.K.
- Wilson, R.M., Elliott, J.C., and Dowker, S.E.P. (1999) Rietveld refinement of the crystallographic structure of human dental enamel apatites. *American Mineralogist*, 84, 1406–1414.

MANUSCRIPT RECEIVED OCTOBER 8, 2003

MANUSCRIPT ACCEPTED MAY 3, 2003

MANUSCRIPT HANDLED BY BRIGITTE WOPENKA